Nanoparticle-controlled glassy dynamics in nematogen-based nanocolloids

Aleksandra Drozd-Rzoska, Szymon Starzonek,* and Sylwester J. Rzoska
Institute of High Pressure Physics of the Polish Academy of Sciences, ul. Sokołowska 29/37, 01-142 Warsaw, Poland

Samo Kralj
Faculty of Natural Sciences and Mathematics, University of Maribor, Koroska 160, 2000 Maribor, Slovenia
and Condensed Matter Physics Department, Jozef Stefan Institute, Jamova 39, 1000 Ljubljana, Slovenia

(Received 31 July 2018; published 31 May 2019)

Results of broad-band dielectric spectroscopy studies in liquid crystal (pentylcyanobiphenyl, 5CB)-based nanocolloids are presented. They reveal the strong impact of $BaTiO_3$ nanoparticles on dynamics and uniaxial ordering. Studies were carried out in an extreme range of temperatures (∼150 K), including the supercooled nematic phase. For the latter, the unique "pretransitional" effect for dielectric constant on approaching solid state is reported. The distortion-sensitive analysis revealed super-Arrhenius dynamics but associated with critical-like behavior. In the isotropic phase, translational-orientational decoupling, unusual for the high temperature dynamic domain, was detected. It can be directly link to heterogeneities—prenematic fluctuations. The model linking the classical Landau-de Gennes approach with Imry-Ma arguments has been developed to discuss experimental results.

DOI: 10.1103/PhysRevE.99.052703

I. INTRODUCTION

Liquid crystalline (LC) nanocolloids are formatted due to the beneficial combination of a liquid crystalline (host) and solid nanoparticles (guest). They are considered as the new domain of the *physics of liquid crystals*, associated with challenging fundamental properties and innovative applications [1–6]. There are nanoparticles (NPs) of different shapes and dimensions, built from different materials (metals, semiconductors, dielectrics) and existing in different phases. Each factor exerts the significant impact on the liquid crystalline host. However, properties of nanocomposites and nanocolloids depend on the type of LC material and its mesophase. Consequently, the extraordinary richness of LCs+NPs composite systems emerges, often with unique metamaterial features. All these have led to the boost of efforts in this new research area [1–6 and Refs. therein]. Within the huge assortment of different nanoparticles, particularly interesting are the ferroelectric ones, which can exhibit anomalously strong impact on the orientational ordering—the basic feature of mesophases for rodlike LC compounds [3–6]. In the *physics of liquid crystals*, the characterization of phase transitions and dynamics of subsequent phases provides a basic reference for theoretical modeling [7–10]. The broadband dielectric spectroscopy (BDS) emerges as a unique tool for such studies: It enables insight into molecular interactions, arrangements of dipole moments polarization, as well as multiscale orientational and translational dynamics [9–13]. However, evidence regarding dynamics and phase transitions and BDS studies is surprisingly limited. The influence of NPs on pretransitional effects was only recently reported [16–26]. Several studies reveal relatively strong impact of ferroelectric particles on static properties of LCs of external field driven structural changes [14,15]. For the evolution of dynamic properties, the Arrhenius or Vogel-Fulcher-Tammann (VFT) description is suggested [4,15,27–31]. However, evidence is the (very) limited temperatures in mesophases. Studies addressing the relationship between orientational and translational dynamics are absent, in practice.

Rasna *et al.* [27] carried out measurements in 5CB + $BaTiO_3$ system focusing on viscoelastic, dielectric, optical properties and phase transitions. The latter was related to the shift of the clearing temperature: 0.63 K increase for 0.01% of NPs was estimated in the DSC scan, although it seems to be poorly visible for assisting dielectric measurements. The addition of NPs (up to 0.4%) notably decreased elastic constants and viscosity. Dielectric studies, focused on the temperature scan at the frequency $f = 1$ kHz, showed up to ca. 13% decrease of $\varepsilon_{\parallel}$ and 4% increase of $\varepsilon_{\perp}$. The specification of experimental conditions reveals typical problems for dielectric tests carried out so far, namely, the measurement capacitor was made from ITO (Indium Tin Oxide) coated glass plates, with additional polymer coating to preserve the alignment and a very thin gap between plates (∼5–13 nm in Ref. [27]). The latter leads to the very high intensity of the electric, namely, assuming the average gap $d = 10$ μm and for the most probable measurement voltage $U = 1$V one obtains $E = 100$ kV/m, i.e., the value for which nonlinear dielectric phenomena are important [13], but omitted in the analysis carried out so far. In Ref. [28] the negligible impact of NPS on the clearing temperature (T^C) was observed. The polymer coating of plats introduces a complex patter of the measurement capacitor. It is notable that in nematogenic MLC6609 LC mixture a huge increase of the clearing temperature reaching 40 K for solely 0.2% of $BaTiO_3$ nanoparticles (50–100 nm) was reported [29]. Urbanski and

*starzoneks@unipress.waw.pl

Lagerwall [30] carried out BDS studies (for $f < 100$ kHz, capacitors gaps $d < 50$ μm) in nematic 5CB doped with gold nanoparticles (3–5 nm). They noted the lack of the impact of NPs on dielectric permittivity but the strong impact of electric conductivity, particularly below a threshold frequency. The impact of silver nanoparticles on dynamics revealed in BDS studies was tested in 70.4 and 70.6 (alkyloxy benzylidene alkylaniline) LCs doped with silver nanoparticles (diameter 5–15 nm), for 1 kHz $< f <$ 1 MHz and the capacitor's gap $d = 25$ μm) [31]. The authors stated that nanoparticles do not contribute to relaxation processes but have the notable impact on the activation energy. The latter was deduced from the suggested Arrhenius dependence of relaxation times, although a more complex super-Arrhenius pattern could be also concluded from the presented results. Probably the first studies focusing on pretransitional effects in liquid crystal-based nanocomposites were carried out in 12CB + $BaTiO_3$ nanocolloid for dielectric constant [14]. 12CB exhibit the isotropic-smectic A (I-SmA) crystal polymorphism. In earlier studies, nanoparticles of diameter 50 nm and bulk gap $d =$ 200 μm between capacitors plates was used. The temperature metric of the discontinuity of the I-SmA transition ΔT^* notably decreases when introducing nanoparticles to the 12CB LC host. The addition of nanoparticles first decreases the dielectric constant by approximately 50% in comparison to pure 12CB. However, for a concentration $x = 0.4\%$ NPs, an increase over 50% was observed. For any concentration of nanoparticles the same value of the specific heat-related critical exponent was obtained. In Ref. [15] the impact of $BaTiO_3$ (diameters between 50 and 200 μm, concentration up to 0.2%) on 5OCB (LC) compound with the isotropic-nematic-crystal mesomorphism was studied. In the isotropic phase the form of the pretransitional effect for dielectric constant did not depend on the presence of nanoparticles, although a weak impact on ΔT^* and the clearing temperature was observed. The subsequent pressure insight revealed a single peak relaxation process in the nematic phase, the Arrhenius-type pressure evolution of the primary relaxation time and the translational orientational decoupling in the nematic phase, what can be linked to the underlying LC structure.

This paper presents BDS studies (up to $f \sim 1$ GHz) in extreme range of temperatures (~150 K) in 5CB (pentylcyanobiphenyl) + $BaTiO_3$ nanocolloids. Notable is the extended range of the mesophase by ca. 30 K, due to the supercooling. The distortion-sensitive analysis revealed the impact of NPs on the orientation of 5CB molecules and the complex dynamics which the clear preference for the critical-like portrayal [32]. In the isotropic phase the uexpected translational-orientational decoupling was found. Notable is the control of dynamics can by the amount of nanoparticles. The experimental evidence is commented by the model linking the Landau-de Gennes phenomenological approach and the Imry-Ma arguments [8,33].

II. METHODOLOGY

A. Experimental

Studies were carried out using the BDS Novocontrol Concept 80 impedance spectrometer enabling the insight into dielectric properties from μHz to 3 GHz frequencies. The flat-parallel capacitor made from gold-coated Invar with diameter $2r = 20$ mm, the gap between plates $d = 200$ μm and the Teflon ring as the spacer was used. Impedance measurements applied $U = 1.5$ V voltage of the measuring field what yielded the intensity $E = 7.5$ kV/m. Tested samples were located in the measurement capacitor in the isotropic liquid phase well above the clearing temperature and then it was linked to the impedance analyzer and cooled to required temperatures. The Quatro Novocontrol temperature control unit enabled the control ± 0.01 K. Pentylcyanobiphenyl (5CB) nematic liquid crystalline compound was synthesized at the Warsaw Military University (WAT, Poland) and carefully purified, with particular attention to the dielectric conductivity. It was carefully degassed immediately prior to measurements. 5CB exhibits the following mesomorphism: *isotropic* $\xrightarrow{T_{IN}=308.3K}$ nematic $\xrightarrow{T_{IN}=296\ K}$ crystal. For presented studies the latter was decreases down to $T_{NS} = 267$ K, due to the careful preparations of sample and measurements capacitors. It is important to recall that 5CB molecule is associated with the permanent dipole moment approximately parallel to the long molecular axis ($\mu = 5$ D) [10]. Mixtures of 5CB and NPs were sonicated with frequency $f = 42$ kHz for a few hours in the isotropic phase until to obtain the homogenous mixture. No sedimentation for at least 24 h was observed and then tested nanocolloids did not contain any additional stabilizing agent. Generally, studies on nanocomposites and nanocolloids based on $BaTiO_3$ explore their ferroelectric nature. However, nanoparticles applied in our studies were spherical with radius $r = 25$ nm and were in the paralectric cubic phase, although the surface with super-paraelectric behavior is also suggested [4].

B. Theoretical approach

We consider spatially homogenous mixtures, where nanoparticles (NPs) are essentially spherical of radius r. The samples are characterized by the volume concentration of NPs

$$c = \frac{N_{NP} v_{NP}}{V}, \tag{1}$$

where N_{NP} stands for the number of NPs within the sample volume V, and $v_{NP} = 4\pi r^3/3$ is the volume of an average nanoparticle. The mass (x) and volume (c) concentrations of NPs are in diluted samples related via

$$x = \frac{c\rho_{NP}}{\rho_{LC}} \tag{2}$$

where ρ_{NP} and ρ_{LC} represent mass densities of NP and LC, respectively. For cases of homogeneously distributed spherical NPs, the average separation between neighboring NPs is given by

$$l_{NP} \sim \left(\frac{4\pi}{3c}\right)^{1/3} r. \tag{3}$$

In our samples, it holds $r \sim 25$ nm and $\rho_{NP}/\rho_{LC} \sim 2$.

We next focus on the LC matrix. We describe the nematic LC ordering at the mesoscopic scale with the nematic uniaxial director field $\vec{n}$ and uniaxial nematic order parameter S. The unit vector $\vec{n}$ points along a local uniaxial orientation of LC

molecules, where the head-to-tail symmetry $\pm\vec{n}$ is assumed. The amplitude of nematic ordering equals $S = 1$ for rigidly aligned LC molecules, and isotropic (ordinary liquid) order is characterized by $S = 0$. The free energy ofc the LC matrix is approximated by $F \sim \int\int\int f_v d^3\vec{r} + N_{\mathrm{NP}} \int\int f_i d^2\vec{r}$, where the first integral runs over the LC body and the second over the LC-NP interfaces. The volume free energy density $f_v = f_c + f_e + f_f$ contribution consists of condensation (f_c), elastic (f_e), and external field (f_f) term. We consider dilute samples for which the NP-LC interactions can be expressed as the sum of interface density contributions f_i over separated particles. We express the free energy contributions using the minimal model, possessing the most essential terms needed for our modeling

$$f_c \sim a_0(T - T^*)S^2 - b_m S^3 + c_m S^4, \tag{4a}$$

$$f_e \sim L_0|\nabla S|^2 - LS^2|\nabla\vec{n}|, \tag{4b}$$

$$f_f \sim -\varepsilon_0 \Delta\varepsilon S(\vec{n}\cdot\vec{E})^2, \tag{4c}$$

$$f_i \sim \frac{wS}{2}[1 - (\vec{n}\cdot\vec{v})^2]. \tag{4d}$$

Here a_0, b_m, c_m are positive material constants, $L > 0$ and $L_0 > 0$ are bare nematic elastic constants. We assume the positive field anisotropy $\Delta\varepsilon = \varepsilon_\parallel - \varepsilon_\perp$, where $\varepsilon_\parallel$ and $\varepsilon_\perp$ measure the dielectric response of LC molecules oriented parallel and perpendicular to the external electric field $\vec{E}$, respectively. The quantity w is the surface interaction constant and determines the local surface normal of a NP-LC interface. By imposing $w > 0$ we assume that NPs enforce the homeotropic anchoring. Note that in this notation the representative Frank elastic constant (K) and the surface anchoring strength (W) read $K \sim LS^2$ and $W \sim wS$. Important length scales of the model are, in addition to geometrically imposed lengths l_{NP} and r, also the nematic order parameter correlation length ξ_n, the external field coherence length ξ_E, and the surface extrapolation length. We express them as

$$\xi_n = \sqrt{K\chi}, \tag{5a}$$

$$\xi_e = \sqrt{\frac{K}{S\varepsilon_0\Delta\varepsilon E^2}}, \tag{5b}$$

$$d_e = \frac{K}{W} = \frac{LS}{w}. \tag{5c}$$

Here $\chi = \left(\frac{\partial^2 f_c}{\partial S^2}\right)^{-1}$, where the second derivative is expressed for S minimizing f_c. For 5CB maximal measured value of the nematic correlation length close to T_{IN} is $\xi_n \sim 20$ nm. Equation (5c) yields $d_c \sim 0.05\mu\mathrm{m} \sim 2r$ for $K \sim 5 \times 10^{-12}$ Jm^{-3} and $W \sim 10^{-4}$ Jm^{-2}. Furthermore, for typical values $E = \mathrm{V}/\mu\mathrm{m}$, $S \sim 0.6$ and $\Delta\varepsilon \sim 10$. Equation (5b) yields $\xi_E \sim 0.3$ μm. The geometrically imposed lengths have the following values: $r \sim 25$ nm, $l_{\mathrm{NP}}(x = 0.001) \sim 20r$, $l_{\mathrm{NP}}(x = 0.01) \sim 10r$.

III. EXPERIMENTAL RESULTS

Examples of the real and imaginary parts of dielectric permittivity spectra for 5CB and its nanocolloid with $BaTiO_3$ are shown in Fig. 1. The dielectric constant (ε_s) constitutes the most classical dielectric characterization of liquid crystalline materials: it is related to the horizontal, frequency-independent domain of the real part of dielectric constant and noted as $\varepsilon'(f) = \varepsilon$ [12]. The static domain slightly shifts in different phases when adding nanoparticles, as seen in Fig. 1. Notwithstanding, the frequency $f \sim 10$ kHz can be selected as the proper one for estimating dielectric constant in each tested case. When increasing the frequency above 1 MHz the value of $\varepsilon'(f)$ gradually decreases since permanent dipole moments cease to follow the electric field [12]. This domain yields the possibility of estimating the relaxation time associated with the orientation: In isotropic liquids it is known as the primary (*alpha, structural*) relaxation time.

When comparing dielectric spectra presented in Fig. 1 probably the most striking difference between 5CB and 5CB+$BaTiO_3$ nanocolloid is visible for $\varepsilon''(f)$ dependence in the solid phase, with the clear emergence of new relaxation processes in the nanocomposite. In the low-frequency domain, which in Fig. 1 occurs for $f < 1$ kHz, translational motions dominate. In this region, $\varepsilon''(f) \propto \omega^{-1}$, which leads to the linear dependence on the log-log scale. It enables the calculation of the DC electric conductivity as $\sigma = \sigma_{\mathrm{DC}} = \omega\varepsilon''(f)$ [12]. In the solid phase, similar behavior takes place, i.e., $\log_{10}\varepsilon''(f) \propto \overline{\omega}\log_{10} f$, but with $\overline{\omega} < 1$. Such behavior can be linked to the anisotropic freezing of molecular motions of molecules within the crystalline network. Figure 2 presents the focused insight of dielectric loss curves in the LC mesophase for 5CB and 5CB+$BaTiO_3$ nanocolloids. They are composed of two parts associated with orientations, the emergence of which is related to the inherent uniaxial symmetry of the nematic phase and the rodlike structure of 5CB molecules [10]. They are: (i) the δ mode, linked to the short molecular axis, and (ii) the *tumbling* mode, related to the long molecular axis.

The *tumbling* mode only slightly manifests in the nematic 5CB and the very strong split of mentioned two modes occurs in 5CB + NPs colloids [9–11]. It is visible that the addition of nanoparticles causes the manifestation of the *tumbling* mode to be much stronger than in pure 5CB, which can reflect the increased freedom for the *tumbling* relaxations if the uniaxial nematic ordering is distorted by the presence of nanoparticles. For any dielectric loss curve the associated relaxation time can be calculated from its peak frequency as $1/\omega_{\mathrm{peak}}$, $\omega_{\mathrm{peak}} = 2\pi f_{\mathrm{peak}}$ [12].

Previous experimental studies gave us insight into the temperature evolution of dielectric constant $\varepsilon(T)$, which can show the dominated arrangement of permanent dipole moments: it is preferably parallel for $d\varepsilon/dT < 0$ and antiparallel for $d\varepsilon/dT > 0$. Generally, dielectric studies in the nematic phase are carried out in nonoriented and oriented samples [7–11]. The latter is focused on the separate detection of the perpendicular $\varepsilon_\perp$ and parallel $\varepsilon_\parallel$ components of dielectric constant, which in a natural way dominate in the uniaxially oriented nematic phase for rodlike LC molecules.

The desired symmetry-breaking orientation can be enforced via a strong enough magnetic field ($B > 1$ T) for 5CB or by covering capacitors plates by some polymeric agents [10]. The latter is associated with the complex pattern of the capacitor and its very small gap ($d \sim$ few μm) [10].

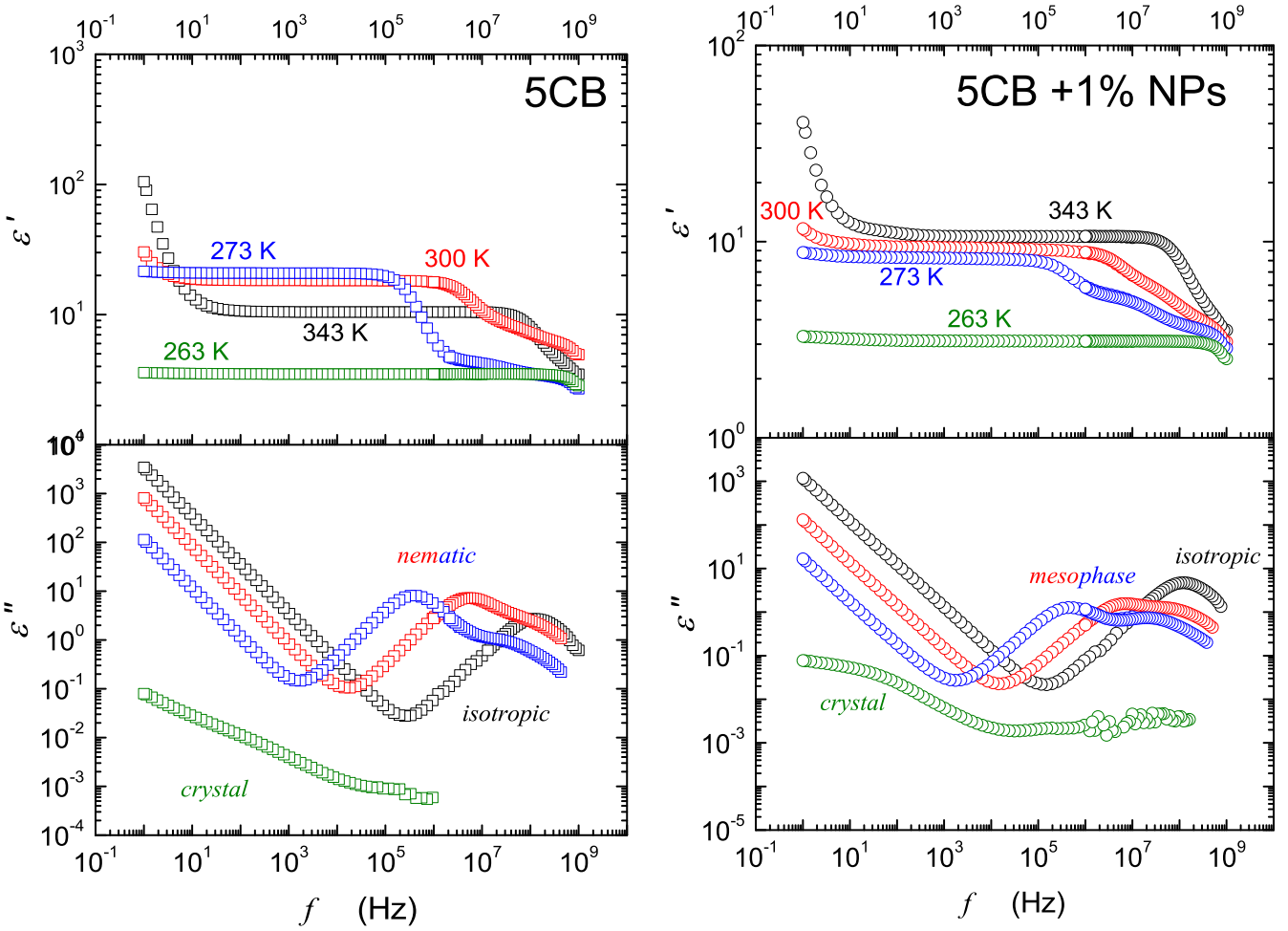

FIG. 1. Dielectric spectra showing frequency dependencies of the real (ε') and imaginary (ε'') parts of dielectric permittivity in the isotropic, nematic and solid phases of 5CB and its colloids with $BaTiO_3$ nanoparticles.

Results presented in this paper were obtained for bulk samples, with $d = 0.2$ mm. The additional weak DC electric field (∼10 V/mm) was applied when passing the isotropic-nematic (I-N) phase transition ($T^C \pm 5$ K). This exogenic impact has no influence on results in the isotropic liquid but in the nematic phase the pattern $\varepsilon(T) = \varepsilon_{\parallel}(T)$ was established, showing the alignment of LC molecules along the direction of the applied electric field $\vec{E}$. This is visible in Fig. 3, where we superpose our experimental results and those by Ratna *et al.* [34] for the oriented via the strong magnetic field 5CB nematic sample. These studies terminate at T_m290 K [34], the standard crystallization temperature for 5CB [12]. However, for results presented in Fig. 3 supercooling down to $T_S \approx T_m - 30$ K in the mesophase was possible. Following Refs. [7,9,10,35,36] one expects that on cooling well below the clearing temperature the almost horizontal behavior of $\varepsilon_{\parallel}(T)$ and $\varepsilon_{\perp}(T)$ takes place: This domain serves as the base for estimating the anisotropy of dielectric constant $\Delta\varepsilon = \varepsilon_{\parallel} - \varepsilon_{\perp}$ being one of the most important characteristics of LC molecular systems [10,36]. However, in Fig. 3 the crossover $d\varepsilon/dT < 0 \rightarrow d\varepsilon/dT > 0$ in the nematic for $T < T_m$ is visible. Adding 0.1% of $BaTiO_3$ nanoparticles yields up to 30% smaller value of dielectric constant than in pure 5CB, but the mentioned pretransitional effect is still manifesting. For 5CB + 1% NPs composite the evolution of $\varepsilon(T)$ approaches to the pattern determined by $\varepsilon_{\perp}(T)$.

In the isotropic phase, temperature changes of dielectric constant may seem to be almost linear in Fig. 3. However, the focused Fig. 4 (for $T > T^C (= T_{IN})$) shows the clear pretransitional behavior associated with the crossover $d\varepsilon/dT < 0 \rightarrow d\varepsilon/dT > 0$. Hence, the addition of NPs to the nematic 5CB changes the enforced uniaxial order. At first sight, there seems to be no pretransitional anomaly in the isotropic liquid phase for results presented in Fig. 3. However, the focused presentation in Fig. 4 clearly shows the pretransitional anomaly associated $d\varepsilon/dT < 0 \rightarrow d\varepsilon/dT > 0$ crossover for approaching the clearing temperature T^C, where one element of symmetry freezes at the isotropic-nematic (I-N) phase transition. The related pretransitional anomaly can portray via the relation [37]

$$\varepsilon(T) = \varepsilon^* + a(T - T^*) + A(T - T^*)^{\phi}, \qquad (6)$$

where $T > T_{\mathrm{IN}} = T^C$, T^C denotes the clearing temperature, $T^* = T^C - \Delta T$, ΔT is the measure of discontinuity of the I-N transition, and (ε^*, T^*) are extrapolated coordinates of the hypothetical (extrapolated) continuous phase transition hidden in the nematic phase. The power exponent $\phi = 1 - \alpha$, where $\alpha = 0.5$ is related to the pretransitional anomaly of the specific heat.

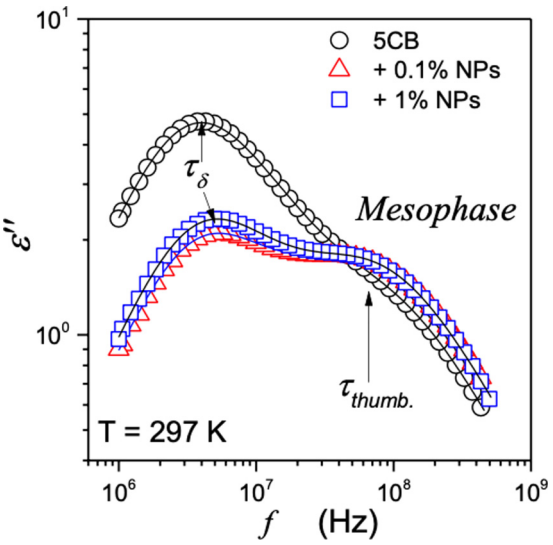

FIG. 2. Dielectric loss curves related to basic relaxation processes in the LC mesophase for the 5CB and 5CB + $BaTiO_3$ nanoparticles composite.

It is worth recalling that such dependence portrays pretransitional effect when approaching the nematic [37], chiral nematic [38], smectic A [39], and smectic E [40] mesophases. This proves that studies of temperature changes of dielectric permittivity detect solely the uniaxial ordering, which is similar for each mentioned LC mesophase. To test the validity of such parametrization as well as for finding optimal values of parameters in Eq. (6) one can apply the transformation of

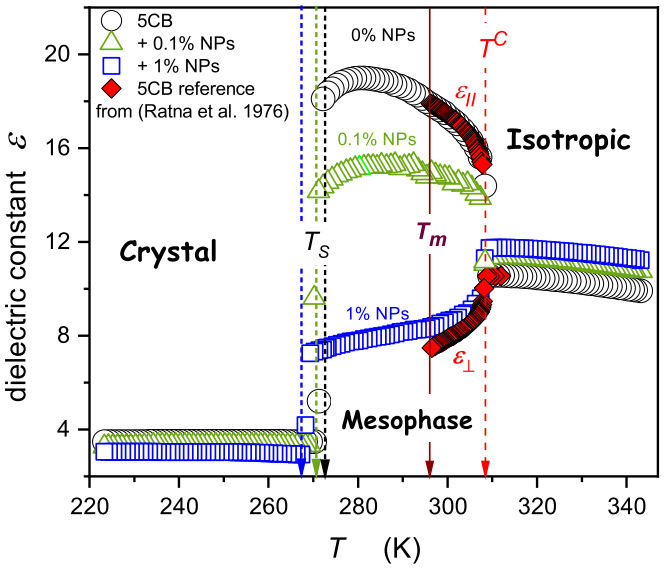

FIG. 3. Temperature dependencies of dielectric constant for 5CB and 5CB+$BaTiO_3$ nanocolloids. The red diamonds are for reference experimental data by Ratna *et al.* [34] for 5CB oriented by the magnetic field. The arrows indicate phase transition temperatures: T^C is for the isotropic-nematic clearing temperature, T_m denotes the standard melting/crystallization temperature for 5CB and T_S is the solidification temperature from the supercooled LC mesophase to the solid state.

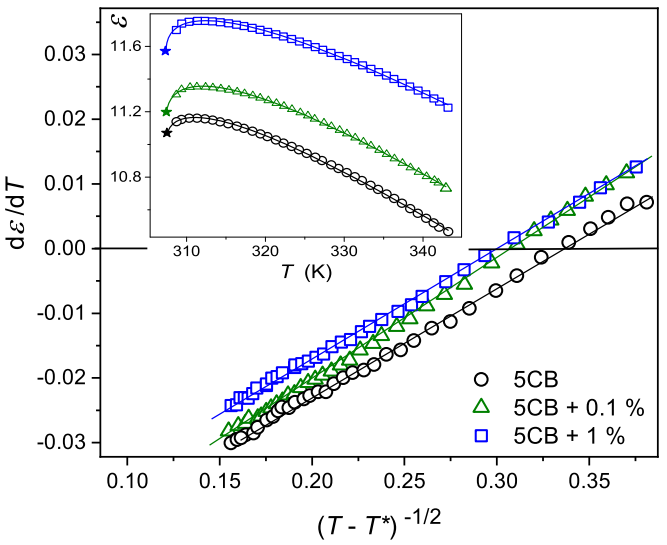

FIG. 4. The behavior of dielectric constant for 5CB and 5CB + $BaTiO_3$ nanocolloids in their isotropic phase. Solid curves parametrizing $\varepsilon(T)$ evolutions are related to Eq. (6), with parameters obtained from the supporting analysis via Eq. (7), the results of which are presented in Fig. 5. Values of parameters are collected in Table I.

experimental data [41]:

$$\frac{d\varepsilon(T)}{dT} = a + A(1-\alpha)(T-T^*)^{-\alpha}. \tag{7}$$

The appearance of the linear dependence for the plot versus $(T-T^*)^{-\alpha}$ yields optimal values of T^* and the exponent α for Eq. (6) and the subsequently, linear regression amplitudes a and A. Results of such analysis are presented in the main part of Fig. 4.

The value of the discontinuity of the I-N phase transition $T^* = 1.5$ K is in fair agreement with earlier estimations from the Kerr effect, light scattering [9,10], and nonlinear dielectric effect [38,42] studies in the isotropic phase of 5CB. The addition of nanoparticles to 5CB increases only the total value of dielectric constant, mainly via the coefficient ε^* in Eq. (6). The pretransitional anomaly is associated with increasing of the volume occupied by prenematic fluctuations—heterogeneities with the antiparallel uniaxial arrangement of permanent dipole moment that causes the qualitatively smaller value of the dielectric constant for the isotropic and fluidlike surrounding.

Broadband dielectric spectra also contain messages related to the orientational and translational dynamics. Figure 5 shows the behavior of key relaxation times related to orientational [$\tau(T)$] and translational ($\tau_\sigma \propto 1/\sigma$) motions. For complex isotropic liquids the dominated structural (*alpha, primary*) relaxation time most often follows the super-Arrhenius (SA) pattern [12,13]:

$$\tau(T) = \tau_0 \exp\left[\frac{E_a(T)}{RT}\right], \tag{8}$$

where $E_a(T)$ displays the apparent activation energy; the simple Arrhenius behavior is characterized by $E_a(T) = E_a$in the given temperature range.

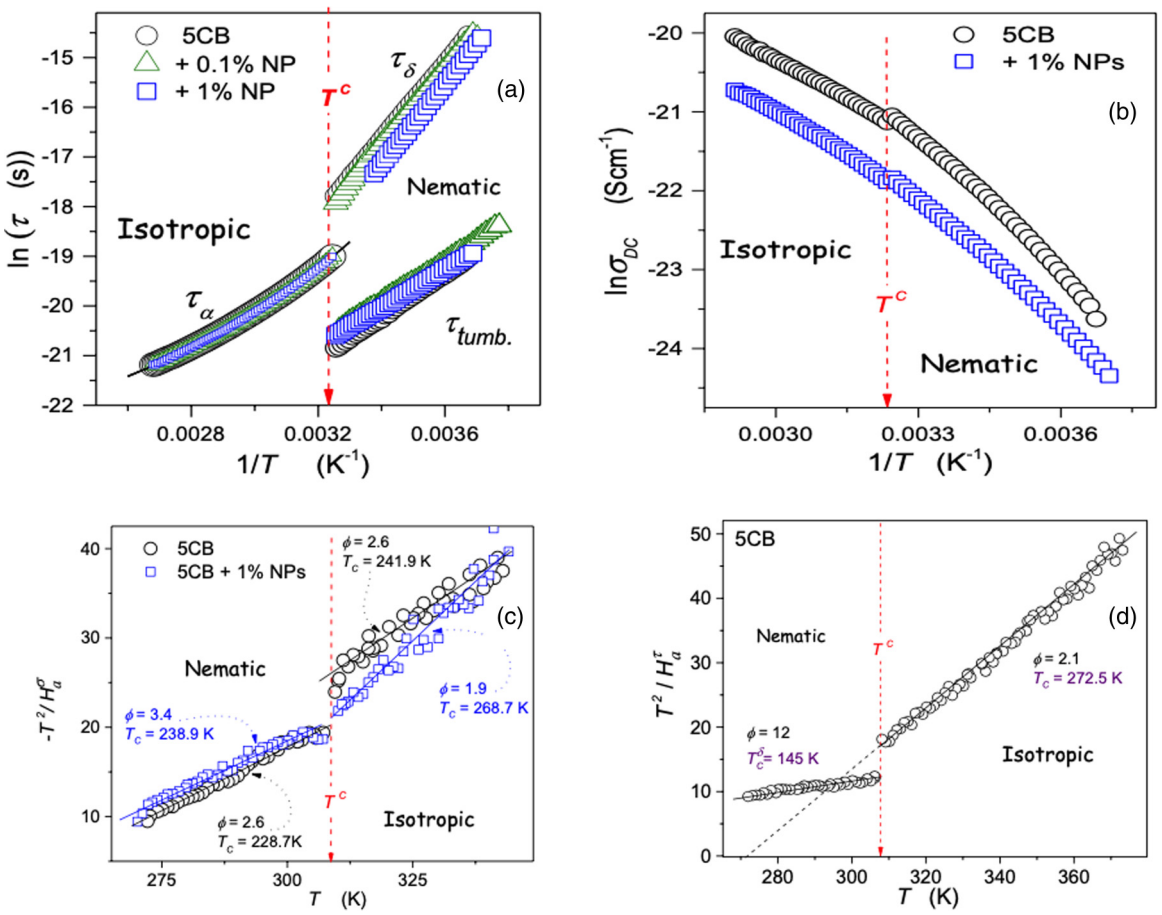

FIG. 5. The Arrhenius plot of the temperature evolution of orientational relaxation times ($\tau = \tau_\alpha, \tau_\delta, \tau_{\text{tumbling}}$) the DC conductivity ($\sigma$) for which the related translational relaxation time $\tau_\sigma \propto 1/\tau$ in 5CB and its nanocolloids with $BaTiO_3$. In Figs. 5(a) and 5(b) the basic Arrhenius relation is manifested via the linear behavior. Panels (c) and (d) show results of the distortion-sensitive analysis based on Eq. (10), showing the clear critical-like behavior [Eq. (9)]. Values of parameters, singular temperatures, and exponents are given in panels (c) and (d).

The unknown general form of $E_a(T)$ dependence causes that the direct application of Eq. (8) for portraying experimental data is not possible and ersatz relations have to be used [12,13]. The most popular one, particularly for glass-forming liquids, is the Vogel-Fulcher-Tammann (VFT) equation, so commonly applied that it is even recalled as the hallmark of the complex glassy dynamics [12,13,32]. It is obtained by substituting in Eq. (8) $E_a(T) = RD_T T T_0/(T - T_0)$, where R is the gas constant, T_0 is the VFT singular temperature, and D_T denotes the fragility strength coefficient. It is worth noting that in glass-forming liquid there are two dynamical domains: the low-temperature domain (LTD) and the high-temperature domain (HTD), separated by the *magic* timescale $\tau(T_B) = 10^{-7\pm1}$ s at the dynamic crossover temperature T_B [43–46]. Each domain is associated with different SA description [32,45], for instance, the VFT equation with two sets of parameters (D_T, T_0) [21]. Notwithstanding, theoretical modeling and the experimental evidence clearly show that in HTD for $T > T_B$ optimal is the critical-like portrayal predicted the mode-coupling theory (MCT) [12,13]:

$$\tau(T) = \tau_0(T - T_C)^{-\phi}, \tag{9}$$

where $T > T_C + 10$ K, T_C is the MCT *critical* temperature: analysis of the experimental data indicates that $T_B \approx T_C$. The exponent $1.5 < \phi < 3$ in different glassy dynamics systems.

For rodlike glass formers, the preference for SA dynamics described by the critical-like behavior occurs also for $T < T_B$ but with the critical-like temperature T_C located below the glass temperature and the exponent $\phi \sim 9$ [47]. Such double critical-like behavior for LTD and HTD was clearly shown for nematic liquid crystals supercooled down to the glass temperature [47–49]. Figures 5(c) and 5(d) present results of the derivative-based and distortion-sensitive analysis which can be derived from the comparison of Eqs. (8) and (9), which can be rearranged to the following dependence [32]:

$$\frac{T^2}{H_a} = \left(\frac{1}{\phi}\right)T - \left(\frac{T_c}{\phi}\right) = aT + b, \tag{10}$$

where the apparent activation enthalpy can be calculated from $\tau(t)$ experimental data via $H_a = R(d\ln\tau/d(1/T) - T)$. For the plot T^2/H_a domains of the validity of the critical-like portrayal manifests via the linear behavior. The subsequent linear regression fit can yield optimal values of the exponent ϕ and the critical temperature T_C, namely, $1/\phi$ and $T_C = b/a$. In the isotropic phase the primary relaxation time follows exactly the same SA pattern [Eq. (10) with $\phi \approx 2.1$ and

$T_C \approx 273$ K] both for 5CB and its nanocolloids, as shown in Fig. 5(a). In the nematic phase two modes of the orientational relaxation are visible (Figs. 1 and 2). Figure 5(a) seems to indicate that for 5CB and 5CB+$BaTiO_3$ nanocolloids δ and *tumbling*-relaxation modes are associated with the basic Arrhenius behavior. Notwithstanding, for nematic 5CB for the δ mode the distortion-sensitive analysis revealed a clear critical-like behavior with the exponent $\phi \approx 12$ [Fig. 5(c)]. For nanocolloids the distortion-sensitive analysis validated the Arrhenius behavior for both relaxation modes in the mesophase. Figure 5(d) shows that the DC electric conductivity and the related translational relaxation time show the clear SA and critical-like behavior in the isotropic liquid and the mesophase. In the isotropic phase values of the *critical exponent* are similar to the ones obtained in MCT model, although it originally omits problems related to the electric conductivity. It is notable that the addition of nanoparticles shifts dynamics towards the SA behavior, which can be expressed also as the increase of the fragility coefficient by 25% for 1% $BaTiO_3$ nanocolloid. The interplay between orientational and translational relaxations is possible via the test based on the Debye-Stokes-Einstein (DSE) dependence [50–52]:

$$\sigma_{DC}\tau_\alpha = \text{const.} \tag{11}$$

Generally, it is expected that in systems with glassy dynamics the crossover from the DSE to the fractional DSE (FDSE) behavior occurs when passing T_B on cooling. The FDSE behavior is related to translational-orientational decoupling described as [50–52]

$$\sigma_{DC}\tau_\alpha^S = \frac{\tau_\alpha^S}{\tau_\sigma} = \text{const.} \tag{12}$$

The crossover DSE ($T > T_B$) $\rightarrow$ FDSE ($T < T_B$) is considered as one of key *universal* features of the glassy dynamics [13,50–53]. It takes place at the empirical apparently universal timescale of the primary relaxation time $\tau(T_B) = 10^{-7\pm1}$ s [43,44,46]. The analysis of experimental data for glass forming liquids showed the fair coincidence between the MCT "critical" temperature and the dynamic crossover temperature, i.e., $T_C \approx T_B$ [53,54]. Figure 6 shows results of the DSE/FDSE focused analysis via the relation $\log_{10}\sigma_{DC} + S\log_{10}\tau_\alpha = \text{const}$ based on Eq. (7).

The isotropic liquid phase of liquid crystals, and then its nanocolloids, can be related to the high-temperature glassy dynamical domain, in which the basic DSE Eq. (11) with the exponent $S = 1$ obeys. For 5CB it is associated with the extrapolated critical temperature located at $T_C \approx T_{IN} - 30$ K [Fig. 5(c)]. However, for 5CB the strong translational-orientational decoupling [Fig. 6(a): $S = 0.77$] despite mentioned expectations occurs as shown in Fig. 6(a). When adding nanoparticles the shift toward the basic DSE pattern takes place, as seen in Figs. 6(b) and 6(c). In the opinion of the authors the unusual translational-orientational decoupling in pure 5CB is associated the strong impact of pretransitional fluctuation in the isotropic liquid: The notable part of molecules is *caged* within prenematic fluctuations, which reduces their translational possibilities and thus can cause the FDSE behavior. The addition of nanoparticles may distort prenematic fluctuation and restore translation of molecules, which can lead to the translational-orientational coupling.

IV. DISCUSSION OF RESULTS

We assume that the samples in our experimental studies are essentially homogeneous. Therefore, for concentrations of $BaTiO_3$ nanoparticles of diameter $d_{NP} = 2r = 50$ nm, the average separations of nearby NPs are estimated by $l_{NP}^{(1)} \sim 0.5\ \mu$m $\sim 10 d_{NP}$ and $l_{NP}^{(2)} \sim 0.24\ \mu$m $\sim 5 d_{NP}$, respectively.

We first consider the experimentally measured dielectric response ε shown in Fig. 3. A part of the dielectric response might be due to dipole moments p_{NP} of NPs. It is not expected to be large because $BaTiO_3$ nanoparticles exhibit the paraelectric ordering. In our diluted samples, their mutual coupling is relatively weak. Consequently, their contribution should exhibit relatively weak temperature variations. However, Fig. 3 demonstrates strong $\varepsilon(T)$ variations, which are therefore dominated by the LC component. We can estimate maximal value of p_{NP} using Eq. (B2) (see Appendix). The contribution of NPs is expected to be visible in the experiments if $\Delta\varepsilon_{NP} \sim 1$. For $c \sim 0.01$ it follows $p_{NP} \sim 10^4 D$. For $r = 25\ \mu$m this implies $P_{NP} \sim p_{NP}/v_{NP} \sim 10^{-3}$ As/m^2.

We next discuss expected interaction of NPs with LC medium and its impact on $\varepsilon(T)$. The response of rodlike uniaxial LC molecules is characterized by $\varepsilon_\parallel$ and $\varepsilon_\perp$ for LC molecules aligned along and perpendicular to $\vec{E}$, respectively. In the case of isotropic distribution of LC molecules the mean dielectric constant value reads $\varepsilon_m = (\varepsilon_\parallel + 2\varepsilon_\perp)/3$ [7,8,10,11]. To explain strong variations in $\varepsilon(T)$ nanoparticles should distort LC medium. The interaction should not be too strong because in this case topological defects would be present. Furthermore, the I-N phase transition temperature shifts should be substantial which is not observed. To explain complexity of observed behaviors we claim that the condition $r/d_e \sim 1$ is realized. For $r \sim 25$ nm this implies $W \sim 10^{-4}$ J/m^2.

We first discuss impact of NPs on the dielectric response in the Isotropic phase. In the isotropic phase the observed changes in dielectric responses of nanocomposites with respect to the bulk LC sample could be due to the following reasons: (i) dipolar contribution of NPs, (ii) contribution of the first layer of LC molecules coating NPs, (iii) contribution of LC molecules in an *outer cloud* enclosing NPs, (iv) contribution of additional dipoles, which arise due to NP induced chemical changes in samples, (v) NPs driven damping of fluctuations in the isotropic phase. In the following, we discuss these potential origins. (i) The NPs could exhibit inherent polarization P_{NP}. This contribution is expected to be weakly T dependent, affecting value of ε^* [see Eq. (6)]. Our analysis described just above suggests that this response is expected to be visible providing $P_{NP} \sim 10^{-3}$ As/m^2. (ii) It is well known that the 1st layer of LC molecules coating the NP's surface is, in general, relatively strongly attached [57]. The corresponding surface induced order parameter is weakly T-dependent. Therefore, these LC molecules would contribute to ε^*. The thickness d of the surface layer is comparable to the characteristic LC molecular length ($\approx$ nm). (iii) The thickness of the *outer cloud* of LC molecules enclosing each NP extends over the nematic order parameter correlation length ξ_n, which is strongly T-dependent. We express the LC contribution to the dielectric response as

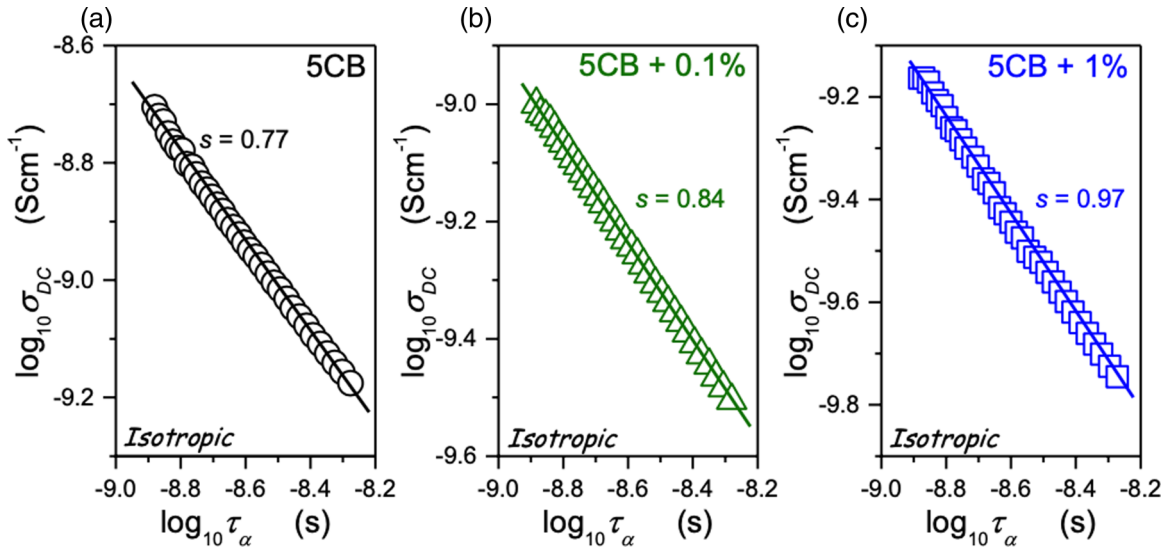

FIG. 6. The log-log plot focusing on the validity of the translational-orientational coupling ($S \approx 1$) and decoupling ($S < 1$): Eqs. (11) and (12). The concentration of $BaTiO_3$ is given in figures.

$\varepsilon_{\rm LC} \approx V_b/V\,\varepsilon_{\rm LC}^{(b)} + V_s/V\,\varepsilon_{\rm LC}^{(s)} + V_c/V\,\varepsilon_{\rm LC}^{(c)}$. Here, $\varepsilon_{\rm LC}^{(b)}$, $\varepsilon_{\rm LC}^{(s)}$, and $\varepsilon_{\rm LC}^{(c)}$ refer to LC responses in bulk, first surface layer of LC molecules coating NPs, and the *outer cloud* contribution. The quantities V_b, $V_s \approx N_{\rm NP} 4\pi r^2 d$, and $V_c \approx N_{\rm NP} 4\pi (r+d)^2 \xi_n$ label volumes occupied by these differently ordered LC molecules, thus $V = V_b + V_s + V_c$. It roughly holds $V_s/V \approx 3cd/r$ and $V_c/V \approx 3c\xi_n/r$. Furthermore, values of $\varepsilon_{\rm LC}^{(b)}$, $\varepsilon_{\rm LC}^{(s)}$, and $\varepsilon_{\rm LC}^{(c)}$ are comparable. For the maximal concentration $c = 0.01$ used in our samples and taking into account maximal value of ξ_n it follows $\varepsilon_{\rm LC} \approx \varepsilon_{\rm LC}^{(b)} + 0.001\varepsilon_{\rm LC}^{(s)} + 0.02\varepsilon_{\rm LC}^{(c)} \approx \varepsilon_{\rm LC}^{(b)}$. Therefore, contributions (ii) and (iii) are relatively small and could not explain the observed dielectric response in the isotropic phase. (iv) NPs could be source of additional dipoles in samples [55,56]. This contribution is also expected to be weakly T-dependent and affecting ε^*. (v) Furthermore, NPs could damp fluctuations [58] in the isotropic phase, effectively acting as a weak ordering field. This weakly temperature-dependent effect could enable stronger response of LC dipoles to the external electric field excitation. The experimental results reveal that in the isotropic phase ε increases with c. Based on our reasoning, we assume that observed changes are either due to contributions (i), (iv), or (v) or a combination of them.

In the nematic phase, the nematic director field becomes frustrated. Namely, the NPs act as seeds for nematic growth. Because of contradicting surface interaction imposed orientations a distorted configuration is formed. Our analysis, discussed in the Appendix, shows that substantial distortions are expected for $x \geqslant 0.001$, which is also consistent with recent experiments on similar samples [56]. Note that in bulk samples one expects $\varepsilon \sim \varepsilon_\parallel > \varepsilon_m$ as it is also observed (see Fig. 3). Therefore, in this case, the nematic director is preferentially aligned along $\vec{e} = \vec{E}/E$. In the sample with $x = 0.001$ one observes substantial drop with respect to the bulk response. This is consistent with our assumption that the nematic ordering becomes frustrated. Consequently, the global degree of nematic order $\langle P_2 \rangle = 1/2\langle(\vec{n}, \vec{e})^2 - 1/3\rangle$, where $\langle \dots \rangle$ stands for spatial average, is expected to decrease on increasing x. However, the mechanism discussed above is not sufficient to explain relatively low values of ε which are observed in the sample with $x = 0.01$. Namely, even in the extreme case, where $\langle P_2 \rangle = 0$, one would expect $\varepsilon \sim \varepsilon_m > \varepsilon_\perp$. But the measurements indicate that values of ε are comparable to $\varepsilon_\perp$. A possible explanation would be that NPs stabilize a nematic structure which is preferentially aligned perpendicular to $\vec{E}$, for which an evident reason does not exist. We claim that in this case, *locking* of dielectric response takes place. Namely, the dipoles of LC molecules experience in addition to the external electric field $\vec{E}$ also the electric field produced by nearby LC molecules. If the latter interaction is much stronger, then an electric dipole does not respond to the external field $\vec{E}$ excitations. To estimate this effect we consider the amplitude of the electric field of an LC molecule generated along its symmetry axis, which we set along the z axis of the Cartesian coordinate system. Therefore, $E_p = p/(2\pi\varepsilon_0 z^3)$, where $p = 5$ D roughly correspond to the electric dipole of a 5CB molecule. Let us focus on the ratio E_p/E where the reference field equals $E = 2 \times 10^3$ V/m. Namely, this field was typically used in our experiments. It follows that $E_p/E > 1$ for distances $z < 52$ nm $\approx d_{\rm NP}$. One sees that the influence range of a dipole is relatively large if its fluctuations are sufficiently suppressed. Note that similar response is typically observed in SmA ordering, where the nematic fluctuations are suppressed due to smectic layers. Therefore, it is very likely that the overall effect of NPs is such that nematic fluctuations are suppressed to the extent that the *locking* effect becomes effective. This effect also explains the sudden drop in ε in the crystal phase. In this case fluctuations of LC molecules are even stronger suppressed, enhancing the locking effect, resulting in a drastic drop in values of ε.

NPs are very likely to introduce disorder into the mixtures, which we believe generates glass-type features present in our measurements. Namely, in the isotropic phase each NP

is surrounded by a *paranematic cloud*. The radius of these *paranematic islands* in the *isotropic sea* is roughly equal to $r + \xi$, where the correlation length is T-dependent. In general, a preferential nematic orientation of these clouds is different. On entering the nematic phase these *clouds* collide and could be trapped in metastable states which is manifested in glassy behavior. Furthermore, the I-N phase transition exhibits the continuous symmetry breaking in orientational ordering. According to the Imry-Ma theorem [33] one of the pivotal theorems of statistical mechanics of disordered systems, even an infinitesimally weak random field-type disorder breaks a long range of the broken phase due to the presence of Goldstone fluctuations. These are inevitable present due to the continuous symmetry breaking. The resulting configuration is expected to exhibit short-range order described by a single characteristic domain length. In our samples, the NP-induced disorder is correlated. Consequently, the imposed disorder is substantially weaker but still strong enough to yield some glass-type features. In the Appendix we illustrate the essential idea of the Imry-Ma [33] theorem adapted to our systems.

Note that for large enough concentrations there is a possibility of phase separation. In particular, even if samples are homogeneous in the isotropic phase the separation could be triggered at the I-N phase transition. Namely, the relative contribution of condensation term [see Eq. (4a)] in nanocomposites is proportional with $(1 - c)$ (i.e., it vanishes in the limit $c = 1$). However, $T^*(c)$ is also affected by NPs. If NPs effectively decrease T_{IN}, then it roughly holds $T^*(c) = T^* - \kappa c$, where κ is a constant. Consequently, when the nematic order is established a free-energy contribution $c(1 - c)\kappa a_0 S^2$ appears, which favours phase separation (i.e., this term is minimized for $c = 1$ or $c = 0$) [59]. However, in our samples we do not find any evidence of this phenomenon.

Finally, we discuss the observed additional relaxation process in the solid state. It might be due to a weakly interacting network of NPs in the liquid crystal host. If NPs modify the surrounding LC ordering then they interact via the distorted nematic director field. Namely, a frustrated nematic director field responds on a geometrically imposed distance over which the frustration is enforced. This is a general consequence of the fact that it can exhibit Goldstone excitations. Consequently, NPs interact in LC host and different network configurations of interacting NPs could exist corresponding to local minima in the respective free energy landscape. Rearrangements in these networks could be the source of the additional relaxation mechanism observed. Note that such changes are observed in mixtures on LCs and aerosols for a relatively low concentration of aerosols in the so-called adaptive network regime [60].

V. CONCLUSIONS

This paper considers the impact of $BaTiO_3$ nanoparticles of radius $r = 25$ nm on the dynamics of 5CB molecules in the temperature interval spanning the isotropic, nematic, and crystal phase. The uniaxial and antiparallel arrangement appears, which is signaled by $d\varepsilon/dT$, both on approaching the nematic phase (orientational freezing) and the solid phase (freezing in the crystalline network). In the nematic the addiction of nanoparticles can crossover the uniaxial ordering from the pattern similar to $\varepsilon_{\parallel}(T)$ to the pattern close to $\varepsilon_{\perp}(T)$. In the isotropic liquid, the observed behavior is associated with the dominant influence of paranematic fluctuation, which is effectively damped by nanoparticles. Consequently, the dielectric constant increases with increasing concentration of NPs. The subsequent studies revealed the notable difference between orientational and translational dynamics in 5CB and 5CB+$BaTiO_3$ nanocolloids. In the isotropic phase, the addition of NPs has no influence on the orientational primary relaxation time but they notably influence the translational relaxation time. In particular, we observe the strong impact of nanoparticle on the translational-orientational coupling strength in the isotropic phase of 5CB. This shows that fluctuations in structural heterogeneities can be responsible for the FDSE behavior, although this requires caging of one type of motions within heterogeneities. Adding of NPs can distort such caging and restore the DSE behavior. Furthermore, experiments reveal that for both orientational and translational relaxations the SA behavior is not associated with the VFT description but with the critical-like, which calls for further investigations. To conclude, we present experimental evidence that adding nanoparticles can crossover dynamics from the (almost) Arrhenius (less fragile) to the SA (more fragile) as well as from DSE to FDSE, i.e., from the translational-orientational decoupling to the coupling regime. Notable are merging possibilities of commenting obtained complex set of experimental results by the model developed on the base linking elements of the Landau-de Gennes model and the Imry-Ma concept.

ACKNOWLEDGMENTS

A.D.R., S.S., and S.J.R. are grateful to the National Science Center (NCN, Kraków, Poland) for the support via Grant No. 2016/21/B/ST3/02203. S.K. acknowledges financial support from the Slovenian Research Agency (Grant No. P1-0099).

APPENDIX A: NANOPARTICLE-INDUCED DISTORTIONS

A nanoparticle immersed in a nematic LC phase is expected to distort the surrounding nematic field if $r/d_e \geqslant 1$. If this condition is fulfilled, then it is very likely that the nematic structure will be distorted. The critical concentration needed for this purpose can be obtained by comparing free energies F of elastically *undistorted* and *distorted* samples for a given concentration c. In the undistorted sample the nematic ordering is spatially homogeneous. Therefore, $\vec{n}$ is aligned along a single symmetry breaking direction. However, the director field spatially varies in the distorted sample. In this estimate dominate role is played by the elastic (F_e) and interface (F_i) free energy contributions. We express the resulting key free energy contribution penalty as $\Delta F^{(\mathrm{state})} = F_e^{(\mathrm{state})} + F_i^{(\mathrm{state})}$, where state $= u$ and state $= d$ label either *undistorted* or *distorted* state. In the undistorted state only surface interaction contribution is present. It holds $\Delta F^{(u)}/V \sim cW/r$. To estimate the free energy penalty of an distorted sample nematic set that homeotropic anchoring is realized (this can be strictly realized in the limit $r/d_e \to \infty$). In this case the interface contribution is negligible. To estimate the elastic penalty we assume that the typical distortion length is given by l_{NP}. It

follows $\Delta F^{(d)}/V \sim K/l_{\rm NP}^2$, $\Delta F^{(u)}/V \sim K/l_{\rm NP}^2$. By imposing $\Delta F^{(d)} = F^{(u)}$ we obtain an estimate for the critical concentration c_c at which a sample becomes significantly elastically distorted:

$$c_c \sim \frac{1}{48\pi^2}\left(\frac{d_e}{r}\right)^3. \tag{A1}$$

For $r/d_e \sim 1$ we obtain $c_c \sim 0.001$. Taking into account $K \sim 5 \times 10^{-12}$ and $r \sim 25$ nm it follows $W \sim 10^{-4}\,\mathrm{J/m^2}$.

APPENDIX B: DIELECTRIC RESPONSE OF ISOLATED DIPOLES

We consider a permanent electric dipole $\vec{p}$ in an external field $\vec{E}$. The average projection of $\vec{p}$ along $\vec{E}$ is determined by $\langle\cos\theta\rangle = \int_{-1}^{1}\cos\theta e^{-W\beta}d\cos\theta/\int_{-1}^{1}e^{-W\beta}d\cos\theta$, where

$$W = -\vec{p}\vec{E}, \tag{B1}$$

$\beta = (k_BT)^{-1}$, and k_B is the Boltzmann constant. In this description we take into account only the coupling with the external electric field and we therefore neglect interaction between different dipoles. The integration yields $\langle\cos\theta\rangle = L(pE\beta)$, where $L(u) = \coth(u) - 1/u$ is the Langevin function. The variation of $\langle\cos\theta\rangle$ monotonously increases with $u = pE\beta$ and becomes saturated in the limit $u \gg 1$. For a relatively small value of u it holds $\langle\cos\theta\rangle \sim u/3 - u^3/45$.

We next estimate impact of dipole moments of NPs on dielectric response within the sample. For this purpose we set in above equations $\vec{p} = \vec{p}_{\rm NP}$, where $p_{\rm NP}$ describes the dipole moment of a ferroelectric nanoparticle. The total polarization of NPs within a sample reads $P_{\rm NP} = \frac{N_{\rm NP}}{V}p_{\rm NP}\langle\cos\theta\rangle = c\frac{p_{\rm NP}}{v_{\rm NP}}\langle\cos\theta\rangle$. In the limit $u \ll 1$ the dielectric contribution of NPs is estimated by

$$\Delta\varepsilon_{\rm NP} \sim \frac{cp_{\rm NP}^2}{3\varepsilon_0 k_B T v_{\rm NP}}. \tag{B2}$$

APPENDIX C: ORIGINS OF THE GLASSY BEHAVIOR

To demonstrate the key idea of the Imry-Ma [33] argument, we complete the elastic and random field-type interactions in the system. Therefore, we assume that NPs effectively introduce a kind of random field. We model the average impact of an individual NP on LC order as

$$\Delta F_i = \iint f_i d^2\vec{r} \sim WP_2(\vec{n}\cdot\vec{e})4\pi r^2, \tag{C1}$$

where $P_2(u) = (3\cos^2 u - 1)/2$ and the unit vector $\vec{e}$ describes the local easy axis preferred by the ith nanoparticle. In this modeling the interface interaction exhibits the minimal value when the director field is aligned along $\vec{e}_i$. In the spirit of the Imry-Ma [33] argument we assume that $\vec{e}_i$ spatially randomly varies and exhibits isotropic probability distribution.

TABLE I. Parameters describing pretransitional effects of dielectric constant in the isotropic phase of 5CB and its nanocolloids with $BaTiO_3$. Parameters are related to Eq. (6) and solid curves in the inset in Fig. 4.

Parameter	5CB	+0.1% NPs	+1% NPs
ε^*	11.010	11.160	11.570
T^* (K)	307.4	307.35	307.5
A (K^{-1})	−0.0418	−0.0426	−0.0370
B ($K^{-1/2}$)	0.160	0.184	0.168
ϕ	0.5	0.5	0.5
ΔT	1.3	1.5	1.6

The Imry-Ma [33] theorem claims that even an infinitesimally weak random-field-type disorder breaks the system into domain-type pattern exhibiting short-range order. The corresponding characteristic domain length ξ_d reveal the compromise between elastic and random-field tendencies. The former favor spatially homogeneous order and the latter tends to align the nematic field along a local random-field-enforced orientation. We consider an average domain of volume V_d and estimate the key free-energy contributions within it. To express the average free-energy elastic $\langle\Delta F_e\rangle$ penalty within the domain we set $\langle|\nabla\vec{n}|^2\rangle \sim 1/\xi_d^2$, and then it follows

$$\frac{\langle\Delta F_e\rangle}{V_d} \sim \frac{K}{\xi_d^2}. \tag{C2}$$

However, the average random-field interaction contribution reads

$$\frac{\langle\Delta F_i\rangle}{V_d} = -\frac{N_d 4\pi r^2 W}{V_d}\langle P_2\rangle, \tag{C3}$$

where N_d stands for the number of NPs within the domain. Because NPs are essentially spatially randomly distributed it holds $c = \frac{N_{\rm NP}v_{\rm NP}}{V} = \frac{N_d v_{\rm NP}}{V}$. Therefore,

$$\frac{\langle\Delta F_i\rangle}{V_d} = \frac{3Wc}{r}\langle P_2\rangle. \tag{C4}$$

Because the distribution of easy axes is isotropic in the limit $\xi_d \to \infty$ it follows $\langle P_2\rangle = 0$. According the central limit theorem for finite domain sizes it holds $P_2 \sim 1/\sqrt{N}$, where $N \sim (\xi_d/l_{\rm NP})^3$ counts number of random field sites within V_d. The size of domains is obtained by balancing elastic and random-field interactions. From the corresponding condition $\langle\Delta F_i\rangle = \langle\Delta F_e\rangle$ we obtain

$$\xi_d \sim \left(\frac{Kr}{3cWl_{\rm NP}^{3/2}}\right)^2. \tag{C5}$$

[1] L. Quien, *Nanoscience with Liquid Crystals. From Self-Organized Nanostructures to Applications* (Springer, Cham, 2014).

[2] M. Urbanski, Liquid Crystals Today **24**, 102 (2016).

[3] I. Muševič, *Liquid Crystals Colloids* (Springer, Cham, 2016).

[4] J. P. F. Lagerwall, G. Scalia, *Liquid Crystals with Nano- and Microparticles. Series in Soft Condensed Matter*, Vol. 7 (World Scientific, Singapore,2017).

[5] Y. Garbovsky and A. Gluschchenko, Nanomaterials **7**, 361 (2017).
[6] I. Musevic, Materials **24**, 11 (2014).
[7] S. Chandrasekhar, *Liquid Crystals* (Cambridge University Press, Cambridge, 1994).
[8] P. G. de Gennes and J. Prost, *The Physics of Liquid Crystals* (Oxford Science Publishing, Oxford, 1995).
[9] S. Kumar, *Liquid Crystals: Experimental Studies of Physical Properties and Phase Transitions* (Cambridge University Press, Cambridge, 2001).
[10] J. Goodby, P. J. Collings, T. Kato, C. Tschierske, H. Gleeson, and P. Raynes (eds.), *Handbook of Liquid Crystals* (Wiley-VCH, Weinheim, 2014).
[11] D. Dunmur, A. Fukuda, and G. Luckhurst, *Physical Properties of Liquid Crystals: Nematics* (INSPEC, Stevenage, 2002).
[12] F. Kremer and A. Schoenhals, *Broadband Dielectric Spectroscopy* (Springer, Berlin, 2002).
[13] K. L. Ngai, *Relaxation and Diffusion in Complex Systems* (Springer, Berlin, 2011).
[14] S. J. Rzoska, S. Starzonek, A. Drozd-Rzoska, K. Czuprynski, K. Chmiel, G. Gaura, A. Michulec, B. Szczypek, and W. Walas, Phys. Rev. E **93**, 020701(R) (2016).
[15] S. Starzonek, S. J. Rzoska, A. Drozd-Rzoska, K. Czuprynski, and S. Kralj, Phys. Rev. E **96**, 022705 (2017).
[16] Y. Reznikov *et al.*, Appl. Phys. Lett. **82**, 1917 (2003).
[17] E. Ouskova *et al.*, Liq. Cryst. **30**, 1235 (2003).
[18] O. Buchnev *et al.*, Mol. Cryst. Liq. Cryst. **422**, 47 (2004).
[19] M. Kaczmarek *et al.*, Nonlinear Opt. Quantum Opt. **35**, 217 (2006).
[20] O. Buchnev *et al.*, JOSA B **24**, 1512 (2007).
[21] H. Atkuri *et al.*, J. Opt. A: Pure Appl. Opt. **11**, 024006 (2009).
[22] O. Kurochkin *et al.*, J. Opt. A: Pure Appl. Opt. **11**, 024003 (2009).
[23] G. Cook *et al.*, Optics Express **18**, 17339 (2010).
[24] G. Cook *et al.*, J. Appl. Phys. **108**, 064309 (2010).
[25] S. Klein *et al.*, Phil. Trans. R. Soc. A **371**, 20120253 (2013).
[26] R. K. Shukla *et al.*, Ferroelectrics **500**, 141 (2016).
[27] M. V. Rasna, L. Cmok, D. R. Evans, A. Mertelj, and S. Dhara, Liq. Cryst. **42**, 1059 (2015).
[28] S. Al-Zangana, M. Turner, and I. Dierking, J. Appl. Phys. **121**, 085105 (2017).
[29] F. Li, O. Buchnev, C. I. Cheon, A. Glushchenko, V. Reshetnyak, Y. Reznikov, T. J. Sluckin, and J. L. West, Phys. Rev. Lett. **97**, 147801 (2006).
[30] M. Urbanski and J. P. F. Lagerwall, J. Mat. Chem. C **4**, 3486 (2016).
[31] K. N. Singh, N. M. Singh, H. B. Sharma, and P. R. Alapati, J. Adv Phys. **8**, 2176 (2015).
[32] A. Drozd-Rzoska and S. J. Rzoska, Phys. Rev. E **73**, 041502 (2006).
[33] Y. Imry and S. Ma, Phys. Rev. Lett. **35**, 1399 (1975).
[34] B. R. Ratna and R. Shashidhar, Pramana **6**, 278 (1976).
[35] A. Drozd-Rzoska, S. J. Rzoska, and K. Czupryñski, Phys. Rev. E **61**, 5355 (2000).
[36] A. Drozd-Rzoska, S. J. Rzoska, and J. Zioło, J. Phys.: Condens. Matter **12**, 6135 (2000).
[37] A. Drozd-Rzoska, S. J. Rzoska, and J. Zioło, Phys. Rev. E **54**, 6452 (1996).
[38] S. J. Rzoska, M. Paluch, S. Pawlus, A. Drozd-Rzoska, J. Jadüyn, K. Czupryñski, and R. Dąbrowski, Phys. Rev. E **49**, 3093 (2003).
[39] A. Drozd-Rzoska, S. J. Rzoska, and J. Zioło, Phys. Rev. E **61**, 5349 (2000).
[40] A. Drozd-Rzoska,S. J. Rzoska, and J. Zioło, Acta. Phys. Polon. **98**, 431 (2000).
[41] A. Drozd-Rzoska, S. Pawlus, and S. J. Rzoska, Phys. Rev. E **64**, 051701 (2001).
[42] A. Drozd-Rzoska, Phys. Rev. E **73**, 022501 (2006).
[43] Q. Zheng and J. C. Mauro, J. Am. Ceram. Soc. **100**, 6 (2017).
[44] V. N. Novikov and A. P. Sokolov, Phys. Rev. E **67**, 031507 (2003).
[45] J. C. Martinez-Garcia, J. Martinez-Garcia, and S. J. Rzoska, J. Chem. Phys. **137**, 064501 (2012).
[46] A. Drozd-Rzoska, S. J. Rzoska, S. Pawlus, J. C. Martinez-Garcia, and J.-L. Tamarit, Phys. Rev. E **82**, 031501 (2010).
[47] A. Drozd-Rzoska, J. Chem. Phys. **130**, 234910 (2009).
[48] A. Drozd-Rzoska, S. J. Rzoska, M. Paluch, S. Pawlus, J. Zioło, P. G. Santangelo, C. M. Roland, K. Czuprynski, and R. Dąbrowski, Phys. Rev. E **71**, 011508 (2005).
[49] S. J. Rzoska, A. Drozd-Rzoska, P. K. Mukherjee, D. O. Lopez, and J. C. Martinez-Garcia, J. Phys.: Condens.: Matter **25**, 245105 (2013).
[50] M. Cutroni, A. Mandanici, and L. de Francesco, J. Non-Cryst. Solids **3017**, 449 (2002).
[51] K. V. Edmond, M. T. Elsesser, G. L. Hunter, D. J. Pine, and E. R. Weeks, Proc. Natl. Am. Soc. **109**, 17891 (2012).
[52] S. Starzonek, S. J. Rzoska, A. Drozd-Rzoska, S. Pawlus, J. C. Martinez-Garcia, and L. Kistersky, Soft Matter **11**, 5554 (2015).
[53] F. Mallamace, C. Branka, C. Corsaro, N. Leone, J. Spooren, S.-H. Chen, and H. E. Stanley, Proc. Natl. Am. Soc. **28**, 22457 (2010).
[54] I. Lelidis, M. Nobili, and G. Durand, Phys. Rev. E **48**, 3818 (1993).
[55] T. Bellini, M. Caggioni, N. A. Clark, F. Mantegazza, A. Maritan, and A. Pelizzola, Phys. Rev. Lett. **91**, 085704 (2003).
[56] C. Kyrou, S. Kralj, M. Panagopoulou, Y. Raptis, G. Nounesis, and I. Lelidis, Phys. Rev. E **97**, 042701 (2018).
[57] G. P. Crawford, R. Stannarius, and J. W. Doane, Phys. Rev. A **44**, 2558 (1991).
[58] S. Kobayashi, T. Miyama, N. Nishida, Y. Sakai, H. Shiraki, Y. Shiraishi, and N. Toshima, J. Display Technol. **2**, 121 (2006).
[59] V. Popa-Nita, P. Schoot, and S. Kralj, Eur. Phys. J. E **21**, 189 (2006).
[60] T. Jin and D. Finotello, Phys. Rev. Lett. **86**, 818 (2001).